Quaternary Research (2024), **117**, 43–53
doi:10.1017/qua.2023.77

Research Article

A prolonged dry Mid-Holocene recorded by Moon Lake in the Tengger Desert, arid and semiarid China

Futao Duan[1], Cheng-Bang An[2], Wei Wang[1], Yongtao Zhao[3] and Aifeng Zhou[2]

[1]Institute of Sci-Tech History and Meteorological Civilization, Research Base for Scientific Cognition and Protection of Cultural Heritage, Nanjing University of Information Science and Technology, Nanjing 210000, China; [2]MOE Key Laboratory of Western China's Environmental Systems, College of Earth and Environmental Sciences, Lanzhou University, Lanzhou 730000, China and [3]Key Laboratory of Desert and Desertification, Northwest Institute of Eco-Environment and Resources, Chinese Academy of Sciences, Lanzhou 730000, China

Abstract

Reconstructing the Mid-Holocene climate change in arid and semiarid areas can help predict regional moisture availability and resultant lake evolution and vegetation changes due to future warming. Here, we present a sediment core (YLH15A) from Moon Lake in the Tengger Desert, arid and semiarid China. Based on robust accelerator mass spectrometry ^{14}C dating and multiproxy analyses (pollen, grain size, elements, and total organic carbon), we reconstructed regional climate changes since 7.6 cal ka BP. The climate was generally dry from 7.6 to 2.8 cal ka BP, as indicated by the dried-up lake, strong aeolian activities, and no vegetation, except for a short-term wet interval between 5.4 and 4.9 cal ka BP. The generally dry climate shifted after 2.8 cal ka BP, which is suggested by expanded steppe desert/steppe and increased vegetation cover; it was also accompanied by lake development, which was likely related to increased groundwater recharge originating from regional precipitation and temporary floods from adjacent mountain areas. Our results reveal a prolonged dry Mid-Holocene and relatively wet Late Holocene that are basically consistent with climatic records from the central–east Asian arid and hyperarid areas. The prolonged dry climate in the arid and hyperarid areas is likely to be related to high evaporation triggered by high temperatures during the Middle Holocene.

Keywords: Moon Lake, Tengger Desert, Mid-Holocene, Arid areas, Prolonged dry climate

(Received 24 June 2023; accepted 4 December 2023)

INTRODUCTION

Reconstructing Holocene climate change is important for predicting and understanding future warming and its regional ecological response (Wanner et al., 2008). In particular, most of the profound climate changes occurred in the Middle Holocene (Steig, 1999; Ruddiman, 2001). However, knowledge of the Mid-Holocene climate changes remains limited, and more high-resolution paleoclimate records from climate-sensitive regions are especially needed. Arid and semiarid China is a highly climate-sensitive area (Reynolds et al., 2007; Huang et al., 2015).

The Holocene optimum in China was characterized by warm temperatures and abundant precipitation, which occurred in the Middle Holocene (8.5–3.0 cal ka BP) (Shi et al., 1994a, 1994b). Most studies suggest that the warm and wet Mid-Holocene was widely recorded in the arid and semiarid areas of China (e.g. Feng et al., 2006; Liu et al., 2018; Feng and Yang, 2019; Wang et al., 2019; Gao et al., 2020; Liu et al., 2021; Ning et al., 2021; Peng et al., 2022; Chen et al., 2023). However, some studies suggest that a dry Mid-Holocene climate has been found in desert regions of arid and semiarid China (such as the Tengger Desert, the Hobq Desert, and the Taklimakan Desert) (see An et al. 2006 and references therein). Wang et al. (2011) further suggest that the Mid-Holocene drought might have prevailed in the central–east Asian arid and hyperarid areas, which may have remained dry for longer periods. Therefore, more work is needed to analyze the variation in Mid-Holocene humidity for the arid and hyperarid areas.

The Tengger Desert, located in arid and semiarid China, is characterized by low precipitation but high evaporation, sparse vegetation, and fragile ecosystems and is sensitive to climate change (Zhu et al., 1980). However, limited research suggests that Holocene climate change in the Tengger Desert is complicated (Herzschuh et al., 2004; Chen et al., 2006; Zhao et al., 2008, 2012a; Li et al., 2009), probably due to the combined effects of the Asian summer monsoon, westerlies, topography, and regional vegetation factors (Li et al., 2011; Zhao et al., 2012a). In this study, we present a sediment core (YLH15A) drilled from Moon Lake in the Tengger Desert to reconstruct the vegetation history, lake hydrology, and associated climate change since the Middle Holocene based on pollen, grain size, elemental, and total organic carbon (TOC) information. Furthermore, regional records were used to determine the climatic characteristics and explore possible mechanisms in the Tengger Desert and even the arid and hyperarid areas during the Middle Holocene.

Corresponding author: Cheng-Bang An; Email: cban@lzu.edu.cn

Cite this article: Duan F, An C-B, Wang W, Zhao Y, Zhou A (2024). A prolonged dry Mid-Holocene recorded by Moon Lake in the Tengger Desert, arid and semiarid China. *Quaternary Research* **117**, 43–53. https://doi.org/10.1017/qua.2023.77

REGIONAL SETTING

Moon Lake, a closed desert lake, is located in the eastern margin of the Tengger Desert, with a lake surface area of ~1.3 km^2 and water depths of 2 to ~4 m (Fig. 1a). Previous studies indicated that many residual lakes in the Tengger Desert are supplied by atmospheric precipitation, near-source ground water, and spring water (Wu, 2009; Lai et al., 2012). The study area is dominated by a dry and temperate continental climate (Luo and Sun, 2005). The neighboring Toudaohu meteorological station indicates that the regional mean monthly temperature is −9.4°C in December and 23.5°C in June, with a mean annual precipitation of 150 mm and a high potential evaporation of 3200 mm (Duan et al., 2018; Fig. 1b). A field survey found that there are few vegetation types around the lake area, mainly xerophytic shrubs, including *Calligonum mongolicum* Turcz., *Hedysarum fruticosum* var. *mongolicum*, *Nitraria sibirica* Pall., *Haloxylon ammodendron* (CA Mey.) Bunge, and *Artemisia ordosica* Krasch. Large numbers of common reed (*Phragmites australis* [Cav.] Trin. ex Steud.) grow in the lake (Fig. 1c). Sandy soil with a low organic matter content, which is not conducive to plant growth and results in low regional vegetation cover, is widely distributed in this region (Luo and Sun, 2005).

MATERIALS AND METHODS

Sampling and dating

In December 2015, a 278-cm sediment core was retrieved from Moon Lake with a Kullenberg-type piston corer, namely, core

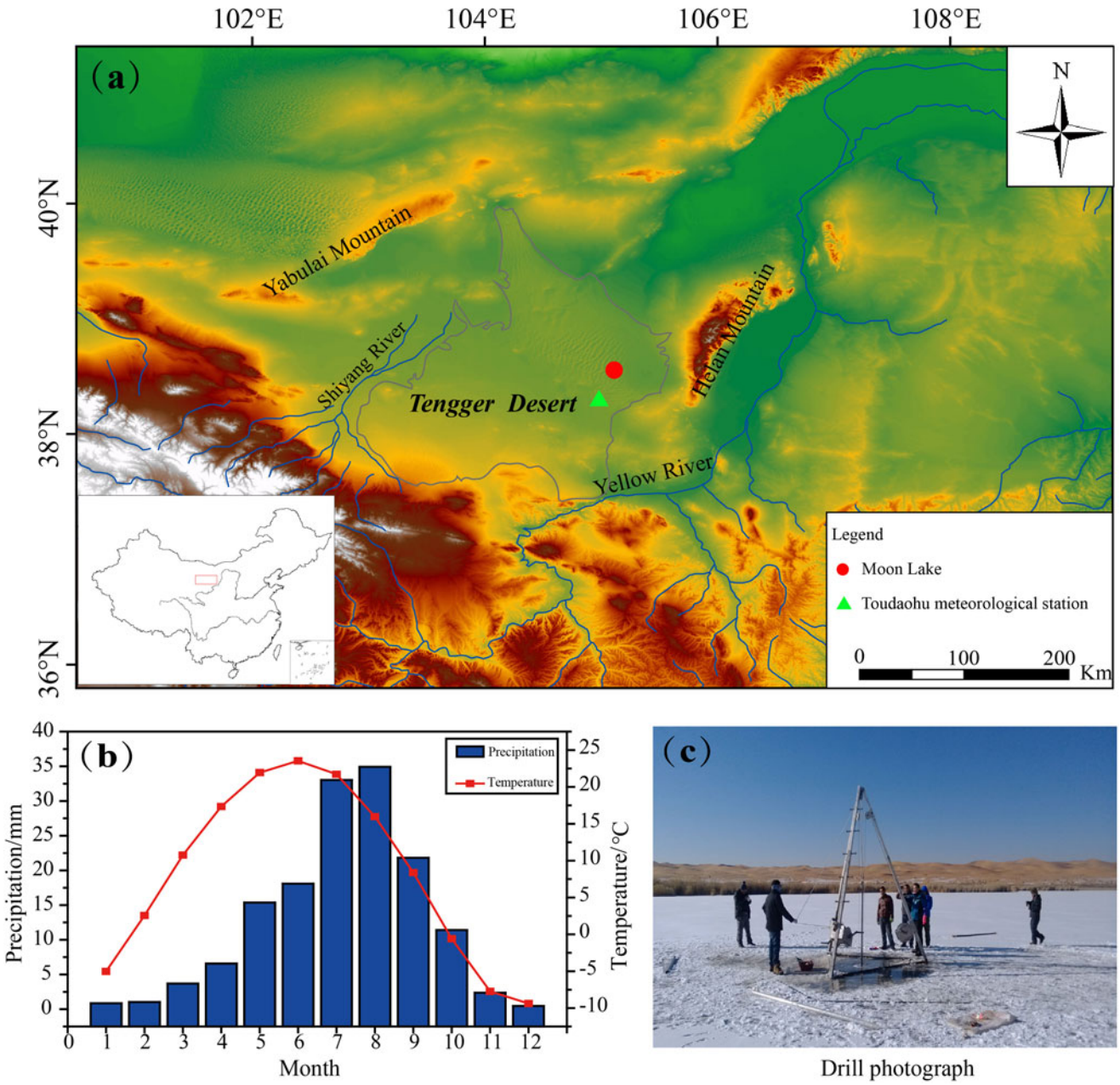

Figure 1. Overview of the study area. (**a**) Map of China noting locations of the Tengger Desert and Moon Lake (sampling site) in the Tengger Desert. (**b**) Mean monthly temperature and precipitation from the Toudaohu meteorological station (1962–2012) (Duan et al., 2018). (**c**) View of the sampling site (YLH15).

https://doi.org/10.1017/qua.2023.77 Published online by Cambridge University Press

YLH15A (38°27.72′N, 105°9.14′ E; 1311 m above sea level) (Fig. 1c). The sediment samples were taken at different intervals for multiproxy analyses (pollen, grain size, TOC, and elements) to explore regional paleoenvironmental changes. In addition, 11 organic samples were selected for accelerator mass spectrometry (AMS) ^{14}C dating at Beta Analytic Inc. (Miami, FL, USA).

Grain size, TOC, and elements

A total of 278 grain-size samples were collected from the YLH15A core at 1 cm intervals for laboratory measurements. The pretreatment procedure followed the description in Peng et al. (2005). The grain-size distribution was measured using a Mastersizer 2000 with a range of 0.02–2000 μm, and the mean measurement error was less than 2%. Based on grain-size distribution data, the grain-size component analysis method (Sun et al., 2002, 2004, 2008) was used to analyze the proportions and origins of different components in the YLH15A core.

Ninety-three samples were collected at 3 cm intervals for TOC content measurements using a TOC analyzer (Elementar, Langenselbold). First, the dried samples were ground and sieved, and then 10% HCl was added into 0.2–0.3 g to remove carbonate. The samples were dried and pressed into pieces for measurement.

The elemental contents of samples at a 1 cm resolution were measured with an Avaatech X-ray fluorescence core scanner. Before core scanning, the split sediment cores were flattened and covered with Ultralene film. The relative variations in the elemental compositions of the sediment core were determined, and then the elemental ratios (e.g., Ca/Ti ratio and Fe/Mn ratio) were calculated. All laboratory work was conducted at the Key Laboratory of Western China's Environmental Systems, Lanzhou University.

Pollen

Sixty-nine samples of approximately 2 g each were selected for pollen analyses at 4 cm intervals. Pollen extraction followed the standard preparation protocol described by Fægri and Iversen (1989). One *Lycopodium*-spore tablet (27,637 grains/tablet) was added to each sample before the chemical treatment to calculate pollen concentrations (Stockmarr, 1971). Pollen identification and counting were performed using pollen atlases of the arid and semiarid areas of China (Xi and Ning, 1994; Wang et al., 1995; Tang et al., 2016) and a Nikon light microscope at 400× magnification. At least 300 grains of terrestrial plant pollen were counted for most samples. A pollen diagram was plotted using Tilia v. 2.02 (Grimm, 2004). CONISS was used for stratigraphically constrained cluster analysis (Grimm, 1987).

RESULTS

Lithology and chronology

The YLH15A sediment core is mainly composed of fine sand and silt, containing almost no clay; in addition, the upper 183 cm of the core also consists of coarse sand (Fig. 2b). The AMS ^{14}C dates of the sediment core were calibrated to calendar years before present (BP) with the Calib v. 7.0 software using the IntCal13 calibration database (Reimer et al., 2013; Table 1). There is an age reversal at depth of 132 cm, which is younger than the upper age. Therefore, the chronology of core YLH15A was established based on 10 AMS ^{14}C dates. Considering that the age of the top of the sediment core is 2015 CE, an age–depth model was generated using a cubic spline interpolator with Bayesian statistical methods (Blaauw and Christen, 2011; Fig. 2a). The chronological sequence of core YLH15A was established based on the weighted mean ages modeled using the Bacon package in R

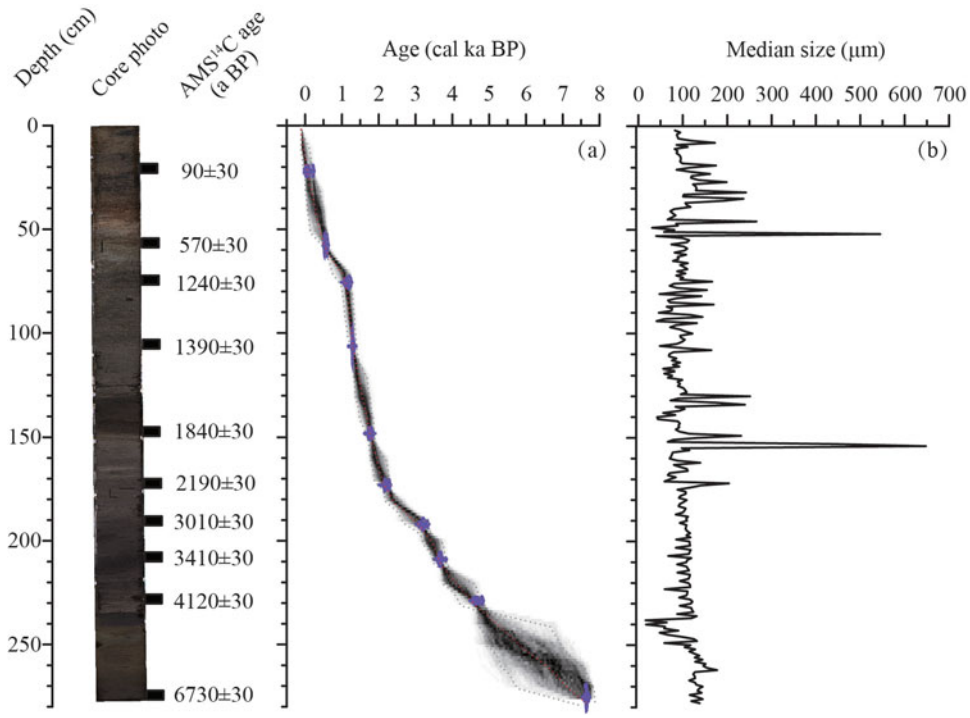

Figure 2. (**a**) Age–depth model and (**b**) median grain-size distribution from sediment core YLH15A.

https://doi.org/10.1017/qua.2023.77 Published online by Cambridge University Press

Table 1. Accelerator mass spectrometry (AMS) ^{14}C dating results from core YLH15A.

Laboratory sample no.	Depth (cm)	Material	$\delta^{13}C$ (‰)	Conventional age (BP)	Calibrated age (cal. yr. BP, 2σ)
Beta414984	21	Bulk sample	−25.7	90 ± 30	265–22
Beta414985	57	Bulk sample	−27.2	570 ± 30	646–527
Beta414986	75	Bulk sample	−26.6	1240 ± 30	1266–1073
Beta414987	106	Bulk sample	−25.5	1390 ± 30	1346–1278
Beta414988	132	Bulk sample	−25.0	1330 ± 30	1301–1184
Beta414989	148	Bulk sample	−24.5	1840 ± 30	1864–1708
Beta414990	173	Bulk sample	−24.6	2190 ± 30	2310–2218
Beta414991	192	Bulk sample	−24.3	3010 ± 30	3334–3077
Beta414992	209	Bulk sample	−24.6	3410 ± 30	3813–3576
Beta414993	229	Bulk sample	−24.3	4120 ± 30	4815–4528
Beta414994	276	Bulk sample	−25.1	6730 ± 30	7660–7521

software, and the bottom age of the YLH15A core was estimated to be 7.6 cal ka BP.

Grain size, TOC, and elemental analyses

All samples of the strata have different sizes and proportions, indicating specific modal size ranges of components with specific origins (Bagnold and Barndorff-Nielsen, 1980). Figure 3 presents two types of statistical plots of the YLH15A core. The grain-size frequency distribution (Fig. 3a) shows the modal size ranges of components with different origins. Three different groups are identified according to the combination of inflections at 38 and 418 μm on the grain-size frequency distribution curve. The group between 0 and 38 μm is short-term suspended dust with a modal size of ~24 μm (Guo et al., 2014; Z.J. Li et al., 2014), which is the typical modal size of the coarse dust component (Sun et al., 2002, 2004, 2008; Yin et al., 2009; Wang et al., 2015). The group between 38 and 418 μm corresponds to the fine sand component with a modal size of ~138 μm, which represents the typical aeolian sand component (e.g., Qiang et al., 2010; Dietze et al., 2014; Z.J. Li et al., 2014; Mou et al., 2018). The >418 μm group with a modal size of ~957 μm corresponds to the coarse sand component. Moreover, the standard deviation for the grain-size class plot (Fig. 3b) shows two peaks observed at grain sizes of 38–418 μm and >418 μm, which represent the two grain-size components that have high variability throughout the sedimentary sequence (Boulay et al., 2003).

Generally, the three grain-size components are characterized by obvious fluctuations above 186 cm, but their variations are relatively stable below 186 cm, except at depths of 243–235 cm. Aeolian sand (38–418 μm) dominates in core YLH15A (mean: 68%; maximum: 95%) and shows the opposite trend relative to coarse dust (<38 μm); the proportion of coarse sand (>418 μm) ranges between 0% and 56% with a mean value of 5% above 186 cm and is accompanied by strong fluctuations, indicating that the sedimentary environment changes greatly. The TOC content is generally low, with a mean value of 1.7. The variations in the Ca/Ti ratio display a similar pattern to TOC, and the trend of changes in the Fe/Mn ratio generally shows an inverse pattern relative to the Ca/Ti ratio. According to the combination of each

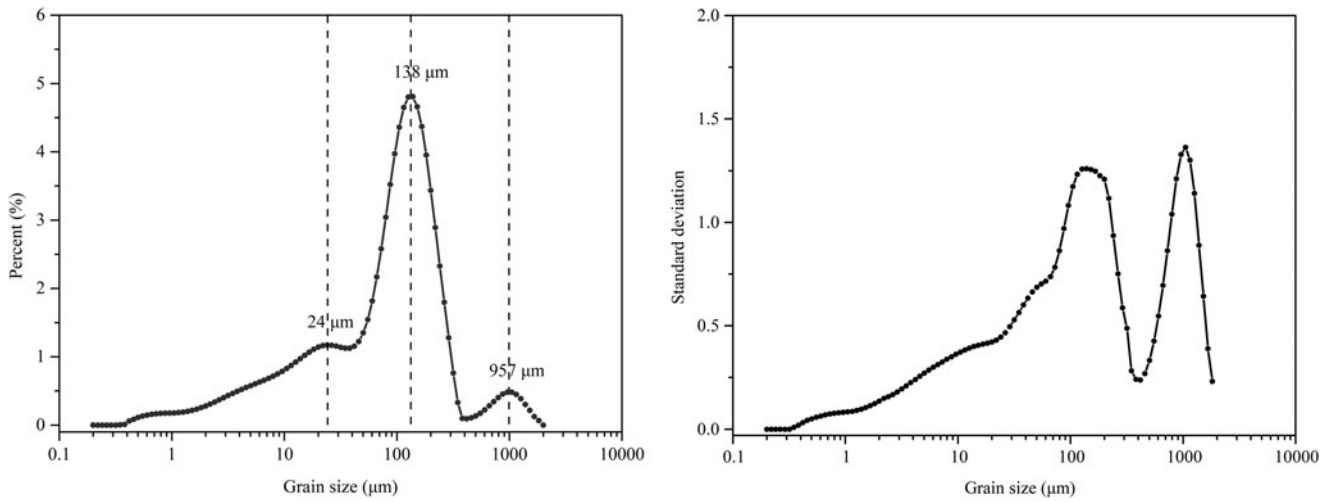

Figure 3. Statistical plots for sediment component analyses: (**a**) mean size distribution of volume frequency for grain-size classes and (**b**) standard deviation of grain-size classes.

https://doi.org/10.1017/qua.2023.77 Published online by Cambridge University Press

proxy, core YLH15A could be divided into four stages, labeled A to D from bottom to top (Fig. 4).

Stage A (278–186 cm, ~7.6 to ~2.8 cal ka BP) is characterized by aeolian sand and coarse dust, and the aeolian sand component generally remains high. Based on the combination of each proxy, this stage is divided into three substages. **Substage A-1** (278–243 cm, ~7.6 to ~5.4 cal ka BP) consists of aeolian sand mixed with minor coarse dust (mean: 17%). Aeolian sand is the dominant component in this stage (mean: 82%). The TOC content (mean: 0.2%) and Ca/Ti ratio (mean: 6.9) are low, while the Fe/Mn ratio reaches a maximum during this stage and maintains a relatively high value (mean: 61). **Substage A-2** (243–235 cm, ~5.4 to ~4.9 cal ka BP) mainly consists of aeolian sand (mean: 56%) and dust components (mean: 44%), and the coarse dust component exhibits a significant increase to a maximum of 76%, while aeolian sand content declines to the lowest value of 24%. TOC content shows a slight increase with a mean value of 3.5%, and the Ca/Ti ratio is relatively low (mean: 24), followed by an obvious increase at 237 cm (~5.0 cal ka BP). The variations in the Fe/Mn ratio show an increase, followed by a significant decline at 239 cm (~5.1 cal ka BP). In **Substage A-3** (235–186 cm, ~4.9 to ~2.8 cal ka BP), aeolian sand dominates and maintains a high content (mean: 70%), and the coarse dust component ranges between 22% and 46%, with a mean value of 30%, which is higher than that of Stage A but lower than that of Stage B. Variations in the Ca/Ti ratio and TOC content generally show similar patterns, with low values (means: 45% and 1.1%, respectively), while the Fe/Mn ratio is high (mean: 59).

In **Stage B** (186–150 cm, ~2.8 to ~1.8 cal ka BP), the proportion of aeolian sand slightly decreases (mean: 63%), but a slight increase is observed in the coarse dust component (mean: 31%). Notably, the coarse sand component starts to appear in this stage and shows strong fluctuations ranging from 0% to 56%, with a mean value of 6%. The Fe/Mn ratio exhibits a significant decrease and remains low (mean: 24). Both the Ca/Ti ratio and TOC content significantly increased.

Stage C (150–73 cm, ~1.8 to ~1.1 cal ka BP) is characterized by aeolian sand and coarse dust mixed with coarse sand deposits, which are accompanied by high variability. Based on the combination of each proxy, this stage is divided into two substages. In **Substage C-1** (150–107 cm, ~1.8 to ~1.3 cal ka BP), the coarse dust components are between 9% and 48%, with a mean value of 29%; the aeolian sand component varies from 36% to 84%, with a mean value of 65%; and coarse sand ranges between 0% and 47%, with a mean value of 6%. The TOC content is generally low (with a mean of 1.7%). The Ca/Ti ratio shows a significant decrease (mean: 28), while the Fe/Mn ratio displays a slight increase (mean: 33). In **Substage C-2** (107–73 cm, ~1.3 to ~1.1 cal ka BP), aeolian sand and the Fe/Mn ratio slightly decrease, while coarse dust and the Ca/Ti ratio generally increase. The TOC content is low but increases to a mean value of 2.8%. Variations in the coarse sand component are more frequent than those in the previous substage.

Stage D (73–0 cm, since 1.1 cal ka BP) still consists of aeolian sand, coarse dust, and coarse sand, but an obvious change occurs at a depth of 50 cm, and the elemental ratios and TOC content also show similar changes. Therefore, this stage is divided into two substages. In **Substage D-1** (73–50 cm, ~1.1 to ~0.5 cal ka BP), the coarse sand component almost disappears, and aeolian sand (mean: 65%) and coarse dust (mean: 32%) dominate the deposits. The Ca/Ti ratios perceptibly increase from 47 to 76, while the Fe/Mn ratios decrease slightly from 28 to 25. The TOC content maintains a low value but increases to a maximum of 3.7. In **Substage D-2** (50–0 cm, since 0.5 cal ka BP), aeolian sand and coarse dust are mixed with coarse sand deposits with high variability. The proportion of coarse dust decreases (mean: 21%), but aeolian sand increases (mean: 69%). The Ca/Ti ratio and TOC content generally decrease, showing an inverse change relative to the Fe/Mn ratio.

Pollen analysis

In the YLH15A core, 20 pollen taxa were identified from 69 samples, including 18 terrestrial pollen taxa and two aquatic pollen taxa. The pollen assemblages are dominated by herb pollen taxa, ranging from 84.7% to 98.7% in abundance, with a mean of 94.5%. The herb pollen types mainly consisted of *Artemisia*, Amaranthaceae, and Poaceae. The abundance of shrubs ranges from 0.8% to 11.7%, with a mean of 3.3%, and mainly consists of *Nitraria* and *Ephedra*. Arboreal pollen accounts for only

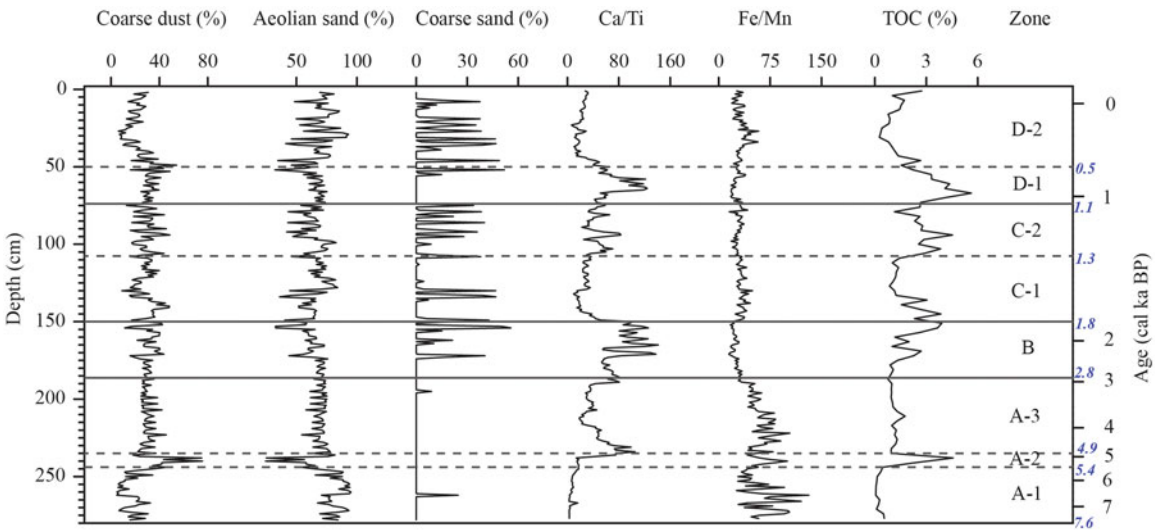

Figure 4. Variation in non-pollen proxies of core YLH15A from Moon Lake. TOC, total organic carbon.

https://doi.org/10.1017/qua.2023.77 Published online by Cambridge University Press

approximately 2.2% of the pollen assemblages (ranging from 0.2% to 8.2%). The terrestrial pollen concentrations range from 0 to 181 grains/g, with a mean of 42 grains/g. Some aquatic pollen types are seen, such as *Typha* and *Pediastrum*. The pollen assemblages are divided into four main zones based on CONISS analysis, and detailed descriptions are as follows (Fig. 5).

In **Stage A** (278–186 cm, ~7.6 to ~2.8 cal ka BP), the study area generally experienced an extremely harsh desert environment with no vegetation cover, which is consistent with the record of no pollen sample found. However, during **Substage A-2** (243–235 cm, ~5.4 to ~4.9 cal ka BP), the pollen assemblages are dominated by *Artemisia* (mean: 45.0%) and Amaranthaceae (mean: 19.3%), with some Poaceae (approximately 5.3%). The pollen concentration reaches a relatively high value during this stage, with a mean of 51 grains/g. The *Artemisia*/Chenopodiaceae (A/C) pollen ratio is approximately 1.8.

In **Stage B** (186–150 cm, ~2.8 to ~1.8 cal ka BP), the pollen assemblage is characterized by *Artemisia*, Asteraceae (excluding *Artemisia*), and Amaranthaceae. A notable feature is the increase in Asteraceae and tree pollen, which reach their maximum values of 8.2% and 40.3%, respectively. However, this stage has an extremely low pollen concentration (mean: 1 grains/g) and insufficient pollen counts.

In **Stage C** (150–73 cm, ~1.8 to ~1.1 cal ka BP), shrub and herb pollen percentages are controlled by *Artemisia* (mean: 51.6%), Amaranthaceae (mean: 27.1%), and Poaceae (mean: 11.9%). In **Substage C-1** (150–107 cm, ~1.8 to ~1.3 cal ka BP), the Amaranthaceae percentage reaches a maximum of 60.3% (mean: 32.3%), and the *Nitraria* percentages are at the highest level for the whole period (up to 10.8%). The A/C ratio is generally low (mean: 1.6) and reaches a minimum of 0.5 at a depth of 134 cm. The pollen concentration starts to increase (mean: 61.6 grains/g). In **Substage C-2** (107–73 cm, ~1.3 to ~1.1 cal ka BP), the *Artemisia* percentage increases (mean: 56.0%), accompanied by an obvious drop in Amaranthaceae (mean: 20.6%). The A/C ratios increase to 2.8. Poaceae pollen significantly increases (up to 21.8%) and remains at a relatively stable value (mean: 14.9%). The pollen concentration increases noticeably (up to 181 grains/g). In addition, the *Typha* percentage increases and accounts for approximately 4.4% during this stage.

In **Stage D** (73–0 cm, since 1.1 cal ka BP), the pollen assemblages resemble those of Stage C, except for the maximized *Artemisia* percentages (up to 74.4%). The A/C ratios are generally high (mean: 4.0). Notably, Poaceae percentages and pollen concentrations generally show a similar fluctuation from high to low since 0.5 cal ka BP (50–0 cm, Substage D-2).

DISCUSSION

Interpretation of the climatic proxies

Grain-size components

The coarse dust component (<38 μm) is aeolian sediment reworked by flowing water, and a higher content indicates that the sediment is closer to the center of the lake and vice versa (Yin et al., 2008, 2009). Therefore, the grain-size component is assumed to reflect fluctuations in the lake level. The aeolian sand component (38–418 μm) is transported by saltation or rolling when strong surface wind occurs (e.g., Qiang et al., 2010; Dietze et al., 2014; Z.J. Li et al., 2014; Mou et al., 2018; Liu et al., 2021). Moreover, this transport of aeolian sand on frozen lakes is associated with strong winds that particularly occur during winter and early spring storms (Sun et al., 2002). Therefore, this component indicates the wind intensity or aeolian activities. The coarse sand component (>418 μm) is alluvial–diluvial sand from the edge of the Tengger Desert and is transported to the lake area by temporary floods triggered by heavy rainfall in mountainous areas (Tsoar and Pye, 1987; Huang et al., 2008; Yin et al., 2009; Dietze et al., 2014; Z.J. Li et al., 2014; Jiang et al., 2021). This situation is common in extremely arid desert-edge areas, where temporary floods caused by heavy rainfall from mountainous areas are an important source of groundwater recharge (Dahan et al., 2008; Greenbaum et al., 2014; Jiang et al., 2021). Therefore, during the period of frequent temporary floods, the increase in groundwater recharge facilitates the development of lakes in desert areas.

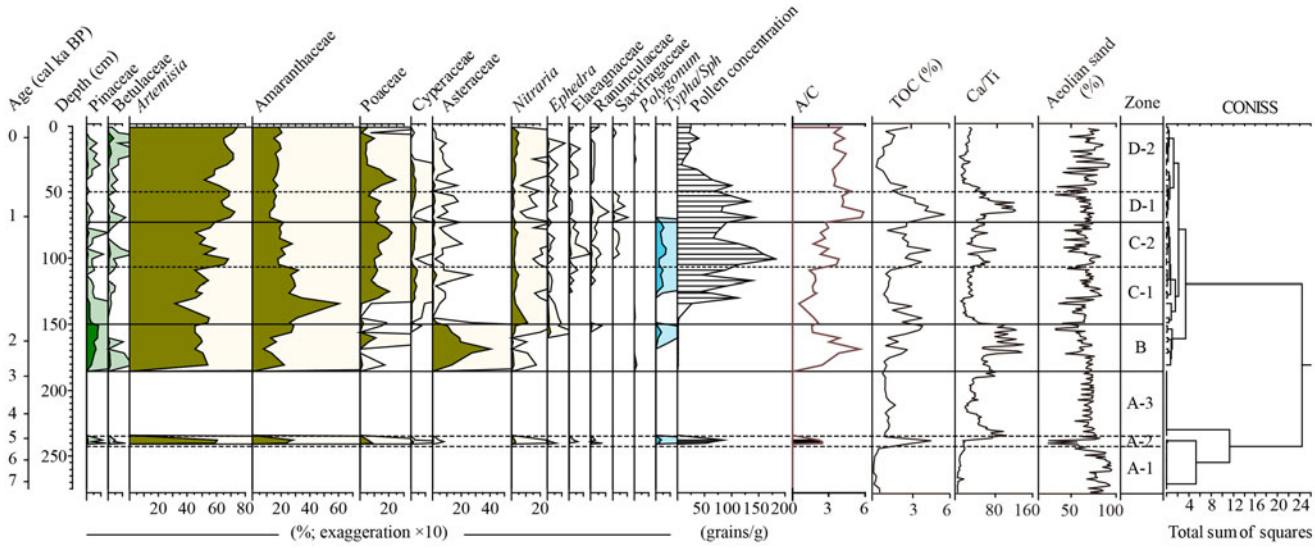

Figure 5. Pollen diagram of the percentage of main pollen taxa and changes in non-pollen proxies (including the total organic carbon [TOC] content, Ca/Ti ratio, and aeolian sand proportion (38–418 μm)) from core YLH15A in Moon Lake.

https://doi.org/10.1017/qua.2023.77 Published online by Cambridge University Press

The Fe/Mn ratio, Ca/Ti ratio, and TOC

The Fe/Mn ratio can be used to reconstruct bottom-water oxygenation in lakes; and the ratio increases from the maximum lake depth toward shallower water depths (Naeher et al., 2013). This is likely due to geochemical focusing, a process in which redox-sensitive trace metals are transferred and enriched at greater lake water depths (Schaller and Wehrli, 1996). The Ca/Ti ratio is used to indirectly reflect the proportion of authigenic and terrigenous lake sediments, which is controlled mainly by precipitation/evaporation and the density of vegetation cover in the watershed (Çağatay et al., 2014). Warm and wet conditions may increase the density of vegetation cover in the watershed, which would reduce erosion rates and increase authigenic carbonate precipitation in the lake, resulting in high Ca/Ti values. This is consistent with the high TOC content attributed to increased lake productivity (Kylander et al., 2013).

The A/C ratio

Artemisia (A) and Amaranthaceae (formerly named Chenopodiaceae) (C) are the dominant plant taxa in arid and semiarid regions, and the former requires more water than the latter during the growing season. Previous studies suggest that the A/C ratio can be used to distinguish steppe from desert and to indicate moisture changes in arid and semiarid regions across the world (e.g., El-Moslimany, 1990; Yan, 1991; Cour et al., 1999; Herzschuh et al., 2004; Li et al., 2005; Zhao et al., 2007). Zhao et al. (2012b) further proposed that the A/C ratio can be used only in regions with precipitation <450–500 mm and in steppe, steppe desert and desert areas, but the threshold A/C values for different vegetation types may vary in different regions. In the Alashan Plateau, the A/C ratios are mostly <1 in desert communities, while in the nearby steppes, the A/C ratios are >2.3 (Herzschuh et al., 2004). Therefore, the A/C ratio from Moon Lake can be used to indicate the past vegetation and moisture conditions; high (low) A/C ratios are associated with an increase (decrease) in steppe pollen production, which corresponds to high (low) relative humidity in this study region (Fig. 5).

Paleoclimate changes recorded by Moon Lake

Paleoclimatic evidence from lake hydrology

Based on grain size, elemental ratios, and TOC analysis, the hydrological changes in Moon Lake since the Middle Holocene can be divided into four main stages.

From 7.6 to 2.8 cal ka BP, there may have been a long-term dried-up lake environment. This inference is supported by the higher content of aeolian sand and higher Fe/Mn ratios (Fig. 4), reflecting strong aeolian activities and extremely shallow water depths in the lake region. Therefore, this period is likely characterized by extremely arid climate. With a notable exception, the temporary lake, pond, or wetland environment occurred in the interval of 5.4–4.9 cal ka BP, which is supported by the high content of coarse dust, reflecting that the sediment was deposited closer to the center of the lake and thus reveals an elevated lake level. This is also supported by the high Ca/Ti ratio and high TOC content (Fig. 4), which further suggest relatively wet conditions during this interval.

The lake environment has existed since 2.8 cal yr BP, but has exhibited instability. From 2.8 to 1.8 cal ka BP, slightly decreased aeolian sand and increased TOC content indicate an improved lake environment (Fig. 4) compared with that in the previous period. During the same period, the temporary flood indicated by the coarse sand component caused an increase in groundwater recharge and thus facilitated the development of the lake, which was also inferred from relatively low Fe/Mn ratios and increased coarse dust. Moreover, high Ca/Ti ratios indicate an increase in authigenic carbonate precipitation in the lake, probably resulting from increased regional precipitation.

From 1.8 to 1.1 cal ka BP, a shallow lake environment occurred, as inferred from relatively high Fe/Mn ratios (Fig. 4). However, the lake environment has improved since 1.3 cal ka BP, which is supported by weakened aeolian activities, increased lake productivity, and increased authigenic carbonate precipitation in the lake. Furthermore, the frequent occurrence of temporary floods and the resultant increased groundwater recharge further suggest a relatively humid lake environment.

From 1.1 to 0.5 cal ka BP, the lake expanded under warm and wet conditions, which is supported by significantly increased Ca/Ti ratios and TOC content. However, relatively high Fe/Mn ratios and decreased coarse dust components indicate an obvious decrease in the lake level since 0.5 cal ka BP (Fig. 4). Moreover, stronger aeolian activities revealed by higher aeolian sand proportions have a more significant impact on the declining lake levels, which further suggests a drying climate since 0.5 cal ka BP.

In summary, the lake hydrology and associated climate change in the lake area mainly experienced two stages: before 2.8 cal ka BP, a dried-up lake environment accompanied by stronger aeolian activities reflected generally dry conditions in this region; since 2.8 cal ka BP, lake development and the increased lake level probably resulted from increased groundwater recharge, which originated from regional precipitation and frequent temporary floods from adjacent mountain areas.

Paleoclimatic evidence from the vegetation history

According to our pollen analysis, desert and desert steppe vegetation has dominated the landscape of the lake region since the Middle Holocene. In general, most pollen represents plants growing in the lake region, but tree pollen and Asteraceae pollen were probably growing in the surrounding mountains at some distance. Detailed descriptions are presented in the following paragraphs.

From 7.6 to 5.4 cal ka BP, desert environment with no vegetation cover prevailed, which is also evidenced by an extremely high aeolian sand deposit content. From 5.4 to 4.9 cal ka BP, this lake region was covered by steppe desert vegetation, which was dominated by *Artemisia*, Amaranthaceae, and Poaceae. The relatively high A/C ratios suggest a moderate moisture availability (Zhao et al., 2012b), which increases vegetation cover. However, the desert landscape prevailed again from 4.9 to 2.8 cal ka BP, similar to the initial environment.

During 2.8–1.8 cal ka BP, a dry desert/steppe desert landscape developed with scarce vegetation cover, which was dominated by *Artemisia*, Asteraceae, and Amaranthaceae. Asteraceae pollen at the YLH15A core likely comes from *Ajania fruticulosa* based on our vegetation investigation in the field; it is widespread in gravel valleys in desert and steppe desert regions (Wang, 1988). Therefore, the abrupt increase in Asteraceae pollen during this period might suggest the expansion of *A. fruticulosa* in the floodplain after flooding from the mountains, with flooding also supported by an increase in tree pollen (Fig. 5). A similar situation also occurs in Qingtu Lake (Zhao et al., 2008). Moreover, the extremely low vegetation cover was probably related to the joint effects of an arid climate and enhanced human activities. The number of archaeological sites from the Alashan Plateau, particularly sites dating to the Qin and Han dynasties (corresponding

https://doi.org/10.1017/qua.2023.77 Published online by Cambridge University Press

to ~2.2 to ~1.8 cal ka BP), has increased dramatically (Guo, 2003; An, 2022), supporting the speculation about low vegetation cover caused by strong human activities.

From 1.8 to 1.1 cal ka BP, desert steppe and steppe desert dominated by *Artemisia*, Amaranthaceae, and Poaceae developed successively in the lake region. The significant increase in Amaranthaceae between 1.7 and 1.6 cal ka BP may be related to human overgrazing activities (Mercuri, 2008; Wen et al., 2010), supported by historical evidence from the states founded by the northern nomadic people (such as Xianbei in the Sixteen States period). Between 1.6 and 1.1 cal ka BP, a high Poaceae content indicates an expansion of steppe over desert and a relatively humid climate (e.g., Li, 1998; Herzschuh et al., 2003; Li et al., 2005; Zhao et al., 2007). Moreover, agricultural policies promoted by the northern Wei dynasty may also be responsible for increases in Poaceae plants. Overall, the lake environment improved, as indicated by the significant increase in vegetation cover during this period (Fig. 5).

From 1.1 cal ka BP to the present, the vegetation landscape was similar to that in the last period. Between 1.1 and 0.5 cal ka BP, higher A/C ratios suggest that the effective moisture availability was favorable for the growth of moisture-demanding plants. However, the significant decreases in the Poaceae percentages and pollen concentrations afterward collectively indicate a drying climate, especially since 0.2 cal ka BP. Moreover, enhanced aeolian activities further reveal the deterioration of the regional environment (Fig. 5). Furthermore, the A/C ratios are still high, which might be caused by increasing water availability to xerophytic plants in the lake area from the aforementioned temporary flood.

In general, the vegetation history and associated climate change in the lake area mainly experienced two stages: before 2.8 cal ka BP, a desert environment with no vegetation cover prevailed, which is also evidenced by a dried-up lake and strong aeolian activities; therefore, the climate of this period was rather arid overall. Since 2.8 cal ka BP, the expansion of desert steppe/steppe desert and increased vegetation cover suggest relatively wet conditions, accompanied by increased lake levels.

Prolonged dry Mid-Holocene in the central–east Asian arid and hyperarid areas

The hydrological changes and vegetation history inferred from Moon Lake suggest the following climatic sequence since the Middle Holocene. The climate was generally dry from 7.6 to 2.8 cal ka BP, as inferred from a dried-up lake and strong aeolian activities, except for a short-term wet episode between 5.4 and 4.9 cal ka BP. The arid climate shifted after 2.8 cal ka BP, as suggested by expanded desert steppe/steppe desert and increased vegetation cover. Meanwhile, it was accompanied by a variable environment, as indicated by changes of pollen types and unstable lake levels during the Late Holocene.

A prolonged dry Mid-Holocene at Moon Lake in the Tengger Desert is also recorded at Lake Zhuyeze (Chen et al., 2006), Lake Juyanze (Hartmann and Wünnemann, 2009) in the Badain Jaran Desert, the Midiwan peat section in the Mu Us Desert (Li et al., 2000, 2003), and Yanhaizi Lake in the Hobq Desert (Chen et al., 2003; Fig. 6). An et al. (2006) further proposed that a prolonged dry Mid-Holocene occurred only in desert regions, but this record cannot be extended to the entire Inner Mongolia Plateau. Recently, the prolonged Mid-Holocene drought has also been extensively documented in central–northern Mongolia (Peck et al., 2002; Fowell et al., 2003; Feng et al., 2007; Prokopenko et al., 2007; An et al., 2008; Wang et al., 2011; Zhang et al., 2012; Fig. 6). These studies suggest that a prolonged drought might have prevailed extensively in the central–east Asian arid and hyperarid areas during the Middle Holocene (Wang et al.,

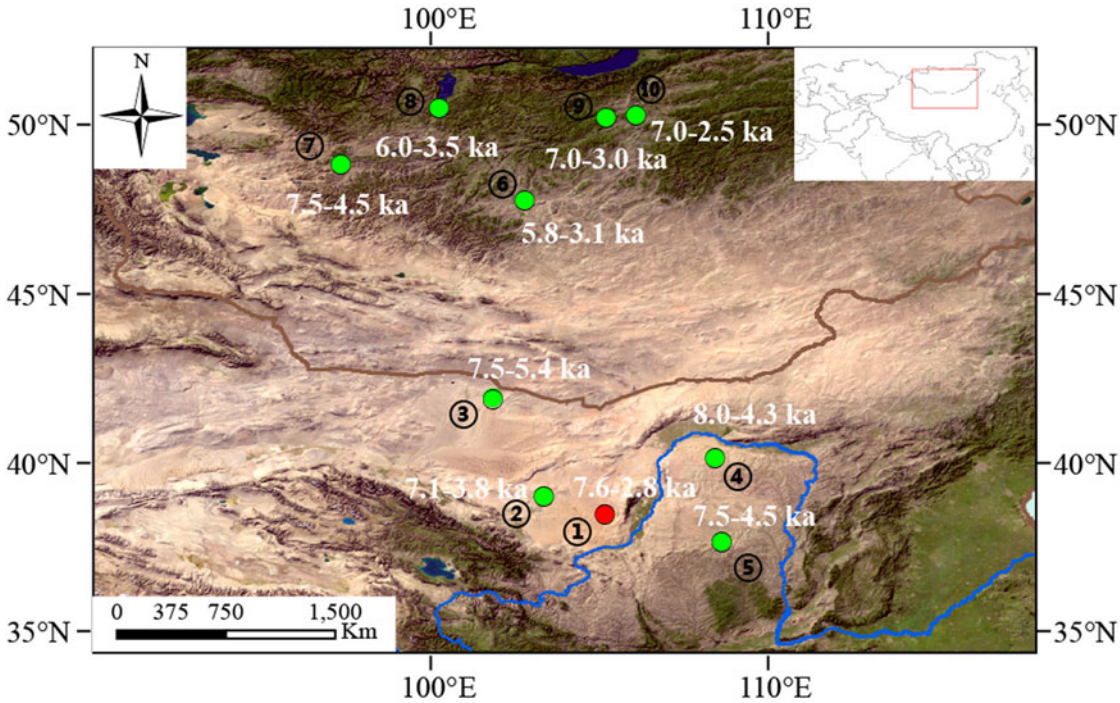

Figure 6. Climatic records of mid-Holocene drought from arid and semi/hyperarid China and Mongolia: 1, Moon Lake (this study); 2, Lake Zhuyeze (Chen et al., 2006); 3, Lake Juyanze (Hartmann and Wünnemann, 2009); 4, Lake Yanhaizi (Chen et al., 2003); 5, Midiwan section (Li et al., 2000, 2003); 6, Ugii Nuur (Wang et al., 2011); 7, Lake Telmen (Fowell et al., 2003); 8, Lake Hovsgol (Prokopenko et al., 2007); 9, Sharmmar section (Feng et al., 2007); 10, Gun Nuur (Zhang et al., 2012).

https://doi.org/10.1017/qua.2023.77 Published online by Cambridge University Press

2011), possibly as a result of the well-documented large-scale temperature rise (Shi et al., 1993). Evaporation triggered by high temperatures might have exceeded the precipitation increase in arid and hyperarid areas, resulting in the increased aridity during the Middle Holocene (Chen et al., 2003; An et al., 2006; Wang et al., 2011). However, the beginning and end of the dry interval could differ in different places due to the different geographic settings (Y. Li et al., 2014; Fig. 6).

During the Late Holocene (since 2.8 cal ka BP), the climate inferred from Moon Lake was relatively wet compared with that in the Middle Holocene, but variations in pollen, grain size, and TOC content indicate an alternation of dry and wet climates (Fig. 5). Similar climatic conditions have also been recorded in the SJC section (since 3.8 cal ka BP) (Chen et al., 2006), Gun Nuur (since 2.5 cal ka BP) (Zhang et al., 2012), Ugii Nuur (since 2.8 cal ka BP) (Schwanghart et al., 2008), the Sharmmar section (since 3.0 cal ka BP) (Feng et al., 2007), and Lake Telmen (since 4.5 cal ka BP) (Fowell et al., 2003). However, further evidence to support a relatively stable and wet Late Holocene is only rarely seen in the central–east Asian arid and hyperarid areas. The uncertain pattern of climate change during the Late Holocene may partly arise from the fact that lakes experienced different degrees of human impact and responded in a nonlinear way due to specific catchment characteristics (Zhang et al., 2012).

CONCLUSIONS

Multiproxy records from Moon Lake in the Tengger Desert revealed lake hydrology, vegetation history, and associated climate change since the Middle Holocene. From 7.6 to 2.8 cal ka BP, this region was characterized by strong aeolian activities, desert landscapes, and a resultant dried-up lake under an extremely arid climate, and higher evaporation could be primarily responsible for the dried-up lake during this period. Since 2.8 cal ka BP, relatively wet conditions were evidenced by vegetation expansion and lake development; furthermore, regional precipitation and temporary floods from adjacent mountain areas recharged the ground water and thus facilitated lake development in desert areas.

These results reveal that Moon Lake experienced a prolonged dry Mid-Holocene and relatively wet Late Holocene that are basically consistent with climatic records from the central–east Asian arid and hyperarid areas, but it is different from either monsoon- or westerly dominated regions and from the East Asian monsoon margin region. More and well-dated Holocene climate records are needed from the core areas of the arid and hyperarid areas to further validate (or contradict) this conclusion.

Acknowledgments. This study was supported by the Natural Science Foundation of Jiangsu Province (no. BK20210656 and no. BK20210658), the National Natural Science Foundation of China (no. 42220104001 and no. 42201169), and the Start-up Foundation for Introducing Talent of NUIST (no. 2021r136).

REFERENCES

An, C.B., 2022. *The Hanhai Sand on the Wanli Ancient Road: Human Activities in the Chinese Desert and Its Adjacent Areas from the Perspective of Environmental Archaeology*. [In Chinese.] Science Press, Beijing, China.

An, C.B., Chen, F.H., Barton, L., 2008. Holocene environmental changes in Mongolia: A review. *Global and Planetary Change* **63**, 283–289.

An, C.B., Feng, Z.D., Barton, L., 2006. Dry or humid? Mid-Holocene humidity changes in arid and semi-arid China. *Quaternary Science Reviews* **25**, 351–361.

Bagnold, R.A., Barndorff-Nielsen, O., 1980. The pattern of natural size distributions. *Sedimentology* **27**, 199–207.

Blaauw, M., Christen, J.A., 2011. Flexible paleoclimate age-depth models using an autoregressive gamma process. *Bayesian Analysis* **6**, 457–474.

Boulay, S., Colin, C., Trentesaux, A., Pluquet, F., Bertaux, J., Blamart, D., Buehring, C., Wang, P., 2003. Mineralogy and Sedimentology of Pleistocene Sediment in the South China Sea (ODP Site 1144). *Proceedings of the Ocean Drilling Program, Scientific Results* **184**, 1–21.

Çağatay, M.N., Öğretmen, N., Damcı, E., Stockhecke, M., Sancar, Ü., Eriş, K.K., Özeren, S., 2014. Lake level and climate records of the last 90ka from the Northern Basin of Lake Van, eastern Turkey. *Quaternary Science Reviews* **104**, 97–116.

Chen, C.T.A., Lan, H.C., Lou, J.Y., Chen, Y.C., 2003. The dry Holocene Megathermal in Inner Mongolia. *Palaeogeography, Palaeoclimatology, Palaeoecology* **193**, 181–200.

Chen, D.X., Lu, R.J., Liu, X.K., Ding, Z.Y., 2023. Holocene vegetation and climate reconstructions from pollen records in the Mu Us Sandy Land, China. *Catena* **220**, 106698.

Chen, F.H., Cheng, B., Zhao, Y., Zhu, Y., Madsen, D.B., 2006. Holocene environmental change inferred from a high-resolution pollen record, Lake Zhuyeze, arid China. *The Holocene* **16**, 675–684.

Cour, P., Zheng, Z., Duzer, D., Calleja, M., Yao, Z., 1999. Vegetational and climatic significance of modern pollen rain in northwestern Tibet. *Review of Palaeobotany and Palynology* **104**, 183–204.

Dahan, O., Tatarsky, B., Enzel, Y., Kulls, C., Seely, M., Benito, G., 2008. Dynamics of flood water infiltration and ground water recharge in hyperarid desert. *Ground Water* **46**, 450–461.

Dietze, E., Maussion, F., Ahlborn, M., Diekmann, B., Hartmann, K., Henkel, K., Kasper, T., Lockot, G., Opitz, S., Haberzettl, T., 2014. Sediment transport processes across the Tibetan Plateau inferred from robust grain-size end members in lake sediments. *Climate of the Past* **10**, 91–106.

Duan, F.T., An, C.B., Zhao, Y.T., Wang, W., Cao, Z.H., Zhou, A.F., 2018. Vegetation and climate history of Anggertu Lake in the Tengger Desert over the last millennium. *Journal of Oceanology and Limnology* **36**, 2166–2180.

El-Moslimany, A.P., 1990. Ecological significance of common nonarboreal pollen: examples from drylands of the Middle East. *Review of Palaeobotany and Palynology* **64**, 343–350.

Fægri, K., Iversen, J., 1989. *Textbook of Pollen Analysis*. 4th ed. Wiley, London, p. 295.

Feng, Y.Y., Yang, X.P., 2019. Moisture sources of the Alashan Sand Seas in western Inner Mongolia, China during the Last Glacial Maximum and mid-Holocene: interpretation from modern analogues, paleoclimatic simulations and geological records. *Journal of Geographical Sciences* **29**, 2101–2121.

Feng, Z.D., An, C.B., Wang, H.B., 2006. Holocene climatic and environmental changes in the arid and semi-arid areas of China: a review. *The Holocene* **16**, 1–12.

Feng, Z.D., Zhai, X.W., Ma, Y.Z., Huang, C.Q., Wang, W.G., Zhang, H.C., Khosbayar, P., Narantsetseg, T., Liu, K.B., Rutter, N.W., 2007. Eolian environmental changes in the Northern Mongolian Plateau during the past 35,000 yr. *Palaeogeography, Palaeoclimatology, Palaeoecology* **245**, 505–517.

Fowell, S.J.B., Hansen, B.C.S., Peck, J.A., Khosbayar, P., Ganbold, E., 2003. Mid to late Holocene climate evolution of the Lake Telmen Basin, North Central Mongolia, based on palynological data. *Quaternary Research* **59**, 353–363.

Gao, Y.H., Li, Z.L., Zhu, R.X., Wang, N.A., 2020. Quantitative reconstruction of Holocene millennial-scale precipitation in the Asian monsoon margin of northwest China, revealed by phytolith assemblages from calcareous root tubes in the Tengger Desert. *Climate Dynamics* **55**, 755–770.

Greenbaum, N., Schwartz, U., Benito, G., Porat, N., Cloete, G.C., 2014. Paleohydrology of extraordinary floods along the Swakop River at the margin of the Namib Desert and their paleoclimate implications. *Quaternary Science Reviews* **103**, 153–169.

https://doi.org/10.1017/qua.2023.77 Published online by Cambridge University Press

Grimm, E.C., 1987. CONISS: a Fortran 77 program for stratigraphically constrained cluster-analysis by the method of incremental sum of squares. *Computers & Geosciences* **13**, 13–35.

Grimm, E.C., 2004. *TILIA and TILIA.GRAPH v.2.0.2*. Illinois State Museum, Springfield.

Guo, F., Sun, D.H., Wamg, F., Li, Z.J., Li, B.F., 2014. Grain-size distribution pattern of the depositional sequence in central Badain Jaran Desert and its genetic interpretation. *Marine Geology & Quaternary Geology* **34**, 165–173.

Guo, S.X., 2003. *Atlas of Chinese Antiquities: Inner Mongolia Autonomous Region Section*. [In Chinese.] Cultural Relics Press, Beijing.

Hartmann, K., Wünnemann, B., 2009. Hydrological changes and Holocene climate variations in NW China, inferred from lake sediments of Juyanze palaeolake by factor analyses. *Quaternary International* **194**, 28–44.

Herzschuh, U., Kürschner, H., Ma, Y.Z., 2003. The surface pollen and relative pollen production of the desert vegetation of the Alashan Plateau, western Inner Mongolia. *Chinese Science Bulletin* **48**, 1488–1493.

Herzschuh, U., Tarasov, P., Wünnemann, B., Hartmann, K., 2004. Holocene vegetation and climate of the Alashan Plateau, NW China, reconstructed from pollen data. *Palaeogeography, Palaeoclimatology, Palaeoecology* **211**, 1–17.

Huang, J.P., Yu, H.P., Guan, X.D., Wang, G.Y., Guo, R.X., 2015. Accelerated dryland expansion under climate change. *Nature Climate Change* **6**, 166–171.

Huang, X.Z., Chen, F.H., Xiao, S., Lv, Y.B., Chen, J.H., Zhou, A.F., 2008. Primary study on the environmental significances of grain-size changes of the Lake Bosten sediments. [In Chinese with English abstract.] *Journal of Lake Sciences* **20**, 291–297.

Jiang, G.L., Nie, Z.L., Liu, Z., Wang, Z., Zhao, H., Yang, J.S., Shen, J.M., 2021. OSL ages and its hydrological implications of alluvial-diluvial deposits from the southern margin of Badain Jaran Desert. *Earth Science* **46**, 1829–1839.

Kylander, M.E., Klaminder, J., Wohlfarth, B., Löwemark, L., 2013. Geochemical responses to paleoclimatic changes in southern Sweden since the late glacial: the Hässeldala Port lake sediment record. *Journal of Paleolimnology* **50**, 57–70.

Lai, T.T., Wang, N.A., Huang, Y.Z., Zhang, J.M., Zhao, L.Q., Xu, M.S., 2012. Seasonal changes of lake in Tengery Desert of 2002. [In Chinese with English abstract.] *Journal of Lake Sciences* **24**, 957–964.

Li, W.Y., 1998. *Quaternary Vegetation and Environment of China*. [In Chinese.] Science Press, Beijing, pp. 1–48.

Li, X.Q., Zhou, W.J., An, Z.S., Dodson, J., 2003. The vegetation and monsoon variations at the desert loess transition belt at Midiwan in northern China for the last 13 ka. *The Holocene* **13**, 779–784.

Li, X.Q., Zhou, W.J., An, Z.S., Dong, G.R., 2000. The palaeovegetation record of monsoon evolution in the desert-loess transition zone for the last 13 kaBP. [In Chinese with English abstract.] *Acta Botanica Sinica* **42**, 868–872.

Li, Y., Wang, N.A., Cheng, H.Y., Long, H., Zhao, Q., 2009. Holocene environmental change in the marginal area of the Asian monsoon: a record from Zhuye Lake, NWChina. *Boreas* **38**, 349–361.

Li, Y., Wang, N.A., Li, Z.L., Zhang, H.A., 2011. Holocene palynological records and their responses to the controversies of climate system in the Shiyang River drainage basin. *Chinese Science Bulletin* **56**, 535–546.

Li, Y., Wang, N., Zhang, C., 2014. An abrupt centennial-scale drought event and mid-Holocene climate change patterns in monsoon marginal zones of East Asia. *PLoS ONE* **9**, e90241.

Li, Y.C., Xu, Q.H., Zhao, Y.K., Yang, X.L., Xiao, J.L., Chen, H., Lu, X.M., 2005. Pollen indication to source plants in the eastern desert of China. *Chinese Science Bulletin* **50**, 1632–1641.

Li, Z.J., Sun, D.H., Chen, F.H., Wang, F., Zhang, Y.B., Guo, F., Wang, X., Li, B.F., 2014. Chronology and paleoenvironmental records of a drill core in the central Tengger Desert of China. *Quaternary Science Reviews* **85**, 85–98.

Liu, X.K, Lu, R.J., Ding, Z.Y., Lyu, Z.Q., Li, Y.Y., Dong, Z.B., 2021. Holocene environmental changes inferred from an aeolian-palaeosol-lacustrine profile in the Mu Us Desert, northern China. *Frontiers in Earth Science* **9**, 799935.

Liu, X.K., Lu, R.J., Du, J., Lyu, Z.Q., Wang, L.D., Gao, S.Y., Wu, Y.Q., 2018. Evolution of peatlands in the Mu Us Desert, Northern China, since the last deglaciation. *Journal of Geophysical Research: Earth Surface* **123**, 252–261.

Luo, J.B., Sun, B.P., 2005. Study on techniques of vegetation restoration in arid region: a case research along the Yueliangh highway in the Tengger Desert, China. [In Chinese with English abstract.] *Journal of Arid Land Resources and Environment* **19**, 205–208.

Mercuri, A.M., 2008. Plant exploitation and ethnopalynological evidence from the Wadi Teshuinat area (Tadrart Acacus, Libyan Sahara). *Journal of Archaeological Science* **35**, 1619–1642.

Mou, X.S., Ma, J., Wang, Y.D., Fan, Y.X., 2018. End-member modeling analysis and test of grain-size distribution: a case from the late Quaternary sediments of Borehole DK-12 in the western Jilantai–Hetao Basin. [In Chinese with English abstract.] *Journal of Palaeogeography* **20**, 489–500.

Naeher, S., Gilli, A., North, R.P., Hamann, Y., Schubert, C.J., 2013. Tracing bottom water oxygenation with sedimentary Mn/Fe ratios in Lake Zurich, Switzerland. *Chemical Geology* **352**, 125–133.

Ning, K., Wang, N.A., Yang, Z.J., Zhang, L.L., Wang, Y.X., Li, Z.L., 2021. Holocene vegetation history and environmental changes inferred from pollen records of a groundwater recharge lake, Badain Jaran Desert, northwestern China. *Palaeogeography, Palaeoclimatology, Palaeoecology* **577**, 110538.

Peck, J.A., Khosbayar, P., Fowell, S.J., Pearce, R.B., Ariunbileg, S., Hansen, B.C.S., Soninkhishig, N., 2002. Mid to Late Holocene climate change in north central Mongolia as recorded in the sediments of Lake Telmen. *Palaeogeography, Palaeoclimatology, Palaeoecology* **183**, 135–153.

Peng, J., Wang, X.L., Yin, G.M., Adamiec, G., Du, J.H., Zhao, H., Kang, S.G., Hu, G.Y., Zheng, Y., 2022. Accumulation of aeolian sediments around the Tengger Desert during the late Quaternary and its implications on interpreting chronostratigraphic records from drylands in north China. *Quaternary Science Review* **275**, 107288.

Peng, Y.J., Xiao, J.L., Nakamura, T., Liu, B.L., Inouchi, Y., 2005. Holocene East Asian monsoonal precipitation pattern revealed by grain-size distribution of core sediments of Daihai Lake in Inner Mongolia of north-central China. *Earth and Planetary Science Letters* **233**, 467–479.

Prokopenko, A.A., Khursevich, G.K., Bezrukova, X.B., Kuzmin, M.I., Boes, X., Williams, D.F., Fedenya, S.A., Kulagina, N.V., Letunova, P.P., Abzaeva, A.A., 2007. Paleoenvironmental proxy records from Lake Hovsgol, Mongolia, and a synthesis of Holocene climate change in the Lake Baikal watershed. *Quaternary Research* **68**, 2–17.

Qiang, M.R., Chen, F.H., Wang, Z.T., Niu, G.M., Song, L., 2010. Aeolian deposits at the southeastern margin of the Tengger Desert (China): Implications for surface wind strength in the Asian dust source area over the past 20,000 years. *Palaeogeography, Palaeoclimatology, Palaeoecology* **286**, 66–80.

Reimer, P.J., Bard, E., Bayliss, A., Beck, J.W., Blackwell, P.G., Bronk Ramsey, C., Buck, C.E., *et al.*, 2013. IntCal13 and Marine13 radiocarbon age calibration curves 0-50,000 years cal BP. *Radiocarbon* **55**, 1869–1887.

Reynolds, J.F., Smith, D.M.S., Lambin, E.F., Turner, B.L., Mortimore, M., Batterbury, S.P.J., Downing, T.E., *et al.*, 2007. Global desertification: building a science for dryland development. *Science* **316**, 847–851.

Ruddiman, W.F., 2001. *Earth's Climate: Past and Future*. W.H. Freeman, New York.

Schaller, T., Wehrli, B., 1996. Geochemical focusing of manganese in lake sediments—an indicator of deep-water oxygen conditions. *Aquatic Geochemistry* **2**, 359–378.

Schwanghart, W., Schütt, B., Walther, M., 2008. Holocene climate evolution of the Ugii Nuur basin, Mongolia. *Advances in Atmospheric Sciences* **25**, 986–998.

Shi, Y.F., Kong, Z.C., Wang, S.M., 1993. Mid-Holocene climates and environments in China. *Global and Planetary Change* **7**, 219–233.

Shi, Y.F., Kong, Z.C., Wang, S.M., Tang, L.Y., Wang, F.B., Yao, T.D., Zhao, X.T., Zhang, P.Y., Shi, S.H., 1994a. Climates and environments of the Holocene megathermal maximum in China. *Science in China* (*Series B*) **37**, 481–493.

Shi, Y.F., Kong, Z.C., Wang, S.M., Tang, L.Y., Wang, F.B., Yao, T.D., Zhao, X.T., Zhang, P.Y., Shi, S.H., 1994b. The climatic fluctuation and important events of Holocene Megathermal in China. *Science in China* (*Series B*) **37**, 353–365.

Steig, E.J., 1999. Mid-Holocene climate change. *Science* **286**, 1485–1487.

Stockmarr, J., 1971. Tablets with spores used in absolute pollen analysis. *Pollen Spores* **13**, 615–621.

https://doi.org/10.1017/qua.2023.77 Published online by Cambridge University Press

Sun, D., Bloemendal, J., Rea, D.K., An, Z., Vandenberghe, J., Lu, H., Su, R., Liu, T., 2004. Bimodal grain-size distribution of Chinese loess, and its palaeoclimatic implications. *Catena* **55**, 325–340.

Sun, D.H., Bloemendal, J., Rea, D.K., Vandenberghe, J., Jiang, F.C., An, Z.S., Su, R.X., 2002. Grain-size distribution function of polymodal sediments in hydraulic and eolian environments, and numerical partitioning of the sedimentary components. *Sedimentary Geology* **152**, 263–277.

Sun, D.H., Su, R.X., Bloemendal, J., Lu, H.Y., 2008. Grain-size and accumulation rate records from Late Cenozoic aeolian sequences in northern China: implications for variations in the East Asian winter monsoon and westerly atmospheric circulation. *Palaeogeography Palaeoclimatology Palaeoecology* **264**, 39–53.

Tang, L., Mao, L., Li, C., Shen, C., Zhou, Z., 2016. *An Illustrated Handbook of Quaternary Pollen and Spores in China*. Science Press, Beijing.

Tsoar, H., Pye, K., 1987. Dust transport and the question of desert loess formation. *Sedimentology* **34**, 139–153.

Wang, F., Sun, D.H., Chen, F.H., Bloemendal, J., Guo, F., Li, Z.J., Zhang, Y.B., Li, B.F., Wang, X., 2015. Formation and evolution of the Badain Jaran Desert, North China, as revealed by a drill core from the desert centre and by geological survey. *Palaeogeography, Palaeoclimatology, Palaeoecology* **426**, 139–158.

Wang, F.X., Qian, N.F., Zhang, Y.L., Yang, H.Q., 1995. *Pollen Flora of China*. 2nd ed. [In Chinese.] Science Press, Beijing.

Wang, J.T., 1988. The steppes and deserts of the Xizang Plateau (Tibet). *Vegetatio* **75**, 135–142.

Wang, W., Liu, L.N., Li, Y.Y., Niu, Z.M., He, J., Ma, Y.Z., Mensing, S.A., 2019. Pollen reconstruction and vegetation dynamics of the middle Holocene maximum summer monsoon in northern China. *Palaeogeography, Palaeoclimatology, Palaeoecology* **528**, 204–217.

Wang, W., Ma, Y.Z., Feng, Z.D., Narantsetseg, T., Liu, K-B., Zhai, X.W., 2011. A prolonged dry mid-Holocene climate revealed by pollen and diatom records from Lake Ugii Nuur in central Mongolia. *Quaternary International* **229**, 74–83.

Wanner, H., Beer, J., Bütikofer, J., Crowley, T.J., Cubasch, U., Flückiger, J., Goosse, H., Grosjean, M., Joos, F., Kaplan, J.O., *et al.*, 2008. Mid- to Late Holocene climate change: an overview. *Quaternary Science Reviews* **27**, 1791–1828.

Wen, R.L., Xiao, J.L., Chang, Z.G., Zhai, D.Y., Xu, Q.H., Li, Y.C., Itoh, S., Lomtatidze, Z., 2010. Holocene climate changes in the mid-high-latitude-monsoon margin reflected by the pollen record from Hulun Lake, northeastern Inner Mongolia. *Quaternary Research* **73**, 293–303.

Wu, Z., 2009. *Sandy Deserts and Their Control in China*. [In Chinese.] Science Press, Beijing.

Xi, Y., Ning, J., 1994. Study on pollen morphology of plants from dry and semidry area in China. *Yunshania* **11**, 119–191.

Yan, S., 1991. The characteristics of Quaternary sporo-pollen assemblage and the vegetation succession in Xinjiang. [In Chinese with English abstract.] *Arid Land Geography* **14**, 1–9.

Yin, Z.Q., Qin, X.G., Wu, J.S., Ning, B., 2008. The multimodal grain-size distribution characteristics and its formation mechanism of lake sediments. *Quaternary Sciences* **28**, 334–342.

Yin, Z.Q., Qin, X.G., Wu, J.S., Ning, B., 2009. The multimodal grain-size distribution characteristics of loess, desert, lake and river sediments in some areas of northern China. [In Chinese with English abstract.] *Acta Sedimentologica Sinica* **27**, 343–351.

Zhang, C.J., Zhang, W.Y, Feng, Z.D., Mischke, S., Gao, X., Gao, D., Sun, F.F., 2012. Holocene hydrological and climatic change on the northern Mongolian Plateau based on multi-proxy records from Lake Gun Nuur. *Palaeogeography, Palaeoclimatology, Palaeoecology* **323–325**, 75–86.

Zhao, Y., Liu, H., Li, F., Huang, X., Sun, J., Zhao, W., Herzschuh, U., Tang, Y., 2012b. Application and limitations of the *Artemisia*/Chenopodiaceae pollen ratio in arid and semi-arid China. *The Holocene* **22**, 1385–1392.

Zhao, Y., Yu, Z.C., 2012a. Vegetation response to Holocene climate change in East Asian monsoon-margin region. *Earth-Science Reviews* **113**, 1–10.

Zhao, Y., Yu, Z.C., Chen, F.H., Ito, E., Zhao, C., 2007. Holocene vegetation and climate history at Hurleg Lake in the Qaidam Basin, Northwest China. *Review of Palaeobotany and Palynology* **145**, 275–288.

Zhao, Y., Yu, Z.C., Chen, F.H., Li, J.A., 2008. Holocene vegetation and climate change from a lake sediment record in the Tengger Sandy Desert, northwest China. *Journal of Arid Environments* **72**, 2054–2064.

Zhu, Z.D., Liu. S., Wu, Z., Di, X.M., 1980. *Deserts in China*. 2nd ed. [In Chinese.] Science in China Press, Beijing, p. 132.

https://doi.org/10.1017/qua.2023.77 Published online by Cambridge University Press